Applied Catalysis B: Environmental 127 (2012) 363–370

Contents lists available at SciVerse ScienceDirect

Applied Catalysis B: Environmental

journal homepage: www.elsevier.com/locate/apcatb

Highly efficient photocatalytic oxidation of sulfur-containing organic compounds and dyes on TiO_2 with dual cocatalysts Pt and RuO_2

Feng Lin[a,b,c], Yongna Zhang[a,b], Lu Wang[a,b], Yuliang Zhang[a,b,c], Donge Wang[a,b], Min Yang[a,b], Jinhui Yang[a,b], Boyu Zhang[a,b,c], Zongxuan Jiang[a,b,*], Can Li[a,b,*]

[a] State Key Laboratory of Catalysis, Dalian Institute of Chemical Physics, Chinese Academy of Sciences, 457 Zhongshan Road, Dalian 116023, China
[b] Dalian National Laboratory for Clean Energy, Dalian 116023, China
[c] Graduate University of Chinese Academy of Sciences, Beijing 100049, China

ARTICLE INFO

Article history:
Received 3 June 2012
Received in revised form 20 August 2012
Accepted 26 August 2012
Available online 5 September 2012

Keywords:
Dual cocatalysts
Sulfur-containing organic compounds
Dyes
Photocatalytic oxidation
Pt–RuO_2/TiO_2

ABSTRACT

Photocatalytic oxidation has been demonstrated to be an effective way for removing organic pollutants *via* a complete mineralization. The removal of sulfur-containing organic compounds in fuel oils and pollutants such as rhodamine B (RhB) and methyl orange (MO) present in the industrial wastewater is highly desired. Here we studied the photocatalytic oxidation of the pollutants on Pt–RuO_2/TiO_2 photocatalyst. We found that TiO_2 co-loaded with noble metal Pt and metal oxide RuO_2 shows the considerably synergistic effect between the two cocatalysts on photocatalytic oxidation activity. This effect has been demonstrated for photocatalytic oxidation of thiophene and successfully extended to photocatalytic oxidation of organic dyes. The high activity is achieved by co-loading less than 0.05 wt% Pt and 0.05 wt% RuO_2 as cocatalysts on TiO_2. ESR measurements give the evidence for that the active oxygen species ($^{\bullet}OH$ and $O_2^{\bullet-}$) generated by photocatalytic processes are involved in photocatalytic oxidation reactions. The reduction cocatalyst Pt and oxidation cocatalyst RuO_2 play significant roles in the photocatalytic oxidation reaction and the co-existing of the dual function cocatalysts is crucial for developing highly active photocatalysts for environmental protection.

1. Introduction

Photocatalytic degradation of harmful organic compounds is of great interest and importance for environmental protection [1–5]. It has been demonstrated that many organic pollutants present in water or air stream can be removed by means of photocatalytic oxidation. Sulfur-containing organic compounds are a class of pollutants in fuel oils and the removal of these pollutants is difficult [6]. However, thiophene, one of the main sulfur-containing compounds in gasoline, is most difficult to oxidize with conventional oxidative desulfurization processes. The inertness of thiophene in the oxidative desulfurization is mainly due to the aromaticity and the low electron density on sulfur atom, which makes the oxidation of thiophene molecule more difficult. Therefore, it is ideal to develop an effective photocatalyst for the removal of sulfur-containing compounds in gasoline *via* photocatalytic oxidation. Additionally, the azo dyes rhodamine B (RhB) and methyl orange (MO) are used globally for coloring textiles. Polluted wastewaters from industry are big environmental issue. Current methods of water purification, such as ozonation and chlorination, use strong oxidants that bring about problems toward the environment. As such, there has been growing interest in environmentally sound materials that can photocatalytically oxidize and degrade chemicals such as RhB and MO, enabling the cleanup of polluted water *via* a far less aggressive approach.

Among the photocatalytic materials, TiO_2 has been extensively used in water treatment and air purification, as well as sterilization [7], sanitation, and remediation applications [8,9]. TiO_2 exhibits high activity and stability and has proven to be an excellent photocatalyst material under UV light exposure [10,11]. It is reported that loading a small amount of noble metals or metal oxides, such as Pt, Ag, NiO, and RuO_2 on TiO_2 [12,13], greatly improves the activity of the photocatalysts [14,15]. However, few researches have been reported for dual cocatalysts effect on the photocatalytic activity of a TiO_2 based photocatalyst for photocatalytic waste oxidation [16–18]. Moreover, the synergistic effect of dual cocatalysts is far less investigated in the photocatalysis for environmental protection.

Herein we studied the photocatalyst TiO_2 co-loaded with less than 0.05 wt% loadings of Pt and RuO_2 (denoted as Pt–RuO_2/TiO_2) used in the photocatalytic oxidation of sulfur-containing organic

* Corresponding authors at: State Key Laboratory of Catalysis, Dalian Institute of Chemical Physics, Chinese Academy of Sciences, 457 Zhongshan Road, Dalian 116023, China. Tel.: +86 411 84379070; fax: +86 411 84694447.
E-mail addresses: canli@dicp.ac.cn (C. Li), zxjiang@dicp.ac.cn (Z. Jiang).
URL: http://www.canli.dicp.ac.cn (C. Li).

0926-3373/$ – see front matter © 2012 Elsevier B.V. All rights reserved.
http://dx.doi.org/10.1016/j.apcatb.2012.08.024

compounds under photo irradiation. We found that TiO_2 co-loaded with noble metal Pt and metal oxide RuO_2 shows the considerably synergistic effect between the two cocatalysts on the photocatalytic oxidation activity. This effect has been demonstrated for the photocatalytic oxidation of thiophene and successfully extended to the photocatalytic oxidation of organic dyes rhodamine B (RhB) and methyl orange (MO). The pollutants (*e.g.*, thiophene, RhB and MO) can be efficiently photocatalytically oxidized on Pt–RuO_2/TiO_2 photocatalyst. The activation of molecular oxygen and pollutant molecule simultaneously takes place on Pt–RuO_2/TiO_2 catalyst for the photocatalytic oxidation reaction. The photocatalysts with both reduction cocatalyst and oxidation cocatalyst offer a more promising approach for the photocatalytic oxidation of pollutants.

2. Experimental

2.1. Catalyst preparation

All chemicals used in these experiments were of analytical reagent grade without further treatment. The photocatalysts were prepared by following two procedures: (1) The loading of metal oxide ($M_{(2)}O_x$) on TiO_2 (Degussa P25) powder was performed by impregnation method. $RuCl_3$, H_2IrCl_6, $Ni(CH_3COO)_2{\cdot}4H_2O$, $Co(CH_3COO)_2{\cdot}4H_2O$, NH_4VO_3, $Mn(CH_3COO)_2{\cdot}4H_2O$ and $Fe(NO_3)_3{\cdot}9H_2O$ were used as the precursors. TiO_2 powder was impregnated in an aqueous solution containing a given amount of the above salts. The solution was then evaporated over a water bath at 50 °C followed by a calcination in air at 400 °C for 0.5 h. (2) The co-loading of metal (M_1) on $M_{(2)}O_x$/TiO_2 was obtained by photo deposition method. As a typical example, H_2PtCl_6 aqueous solution containing a calculated amount of Pt was added to a suspension of RuO_2/TiO_2 dispersed in H_2O (120 mL) and CH_3OH (80 mL). The mixture in inert gas was irradiated with high-pressure mercury lamp (300 W, main wave length 365 nm) for 120 min. The powder was separated by filtration, and then washed several times with distilled water. Finally, the obtained powder was dried at 75 °C under vacuum for 12 h. The photocatalyst, TiO_2 co-loaded with the noble metals M_1 (Pt, Pd, Au, Ni, Cu) and metal oxide $M_{(2)}O_x$ (RuO_2, IrO_2, CoO_x, VO_x, MnO_x, NiO, FeO_x) was denoted as M_1–$M_{(2)}O_x$/TiO_2.

2.2. Catalyst characterization

The prepared samples were characterized by X-ray powder diffraction (XRD) on a Rigaku D/Max-2500/PC powder diffractometer. Each sample powder was scanned using Cu Kα radiation with an operating voltage of 40 kV and an operating current of 200 mA. The scan rate of 5°/min was applied to record the patterns in the range of 8–80° at a step of 0.02°.

UV–Vis diffuse reflectance spectra (UV–Vis DRS) were recorded on a UV-Vis spectrophotometer (JASCO V-550) equipped with an integrating sphere. The morphologies and particle sizes were examined by a Quanta 200 FEG scanning electron microscope.

Transmission Electron Microscopy (TEM) used to examine the particle size and morphology and the images were obtained on a Tecnai G2 Spirit (FEI Company) microscopy with the accelerating voltage of 120 kV. High-resolution Transmission Electron Microscopy (HRTEM) images were obtained on a Tecnai G2 F30 S-Twin (FEI Company) instrument.

ESR signals of radicals trapped by dimethyl pyridine N-oxide (DMPO) were recorded at ambient temperature on a Brucker ESR A200 spectrometer. After bubbling O_2 for 10 min, the samples were introduced into the homemade quartz cup inside the microwave cavity and illuminated with a 300 W Xe lamp (CERAMAX LX-300). The settings for the ESR spectrometer were as follows: center field, 3350.00 G; sweep width, 200 G; microwave frequency, 9.41 GHz; modulation frequency, 100 kHz; power, 10.00 mW. Magnetic parameters of the radicals detected were obtained from direct measurements of magnetic field and microwave frequency.

2.3. Photocatalytic reaction

The photocatalytic oxidation reactions of thiophene were carried out in a Pyrex reaction cell with O_2 bubbled in a constant flow as oxidant. Photocatalyst (1 g L^{-1}) was dispersed in acetonitrile solution containing thiophene ($[\text{sulfur content}]_{\text{initial}}$ = 600 ppm). The suspension was stirred in the dark for 30 min to establish adsorption/desorption equilibrium between the solution and photocatalyst before irradiated by a 300 W Xe lamp (CERAMAX LX-300). The temperature of the reaction solution was maintained at 11 ± 2 °C by a flow of cooling water. And the products and byproducts were analyzed by GC-FPD (Agilent 7890, FFAP column) and GC–MS after separation of the catalyst particles from the reaction system by centrifugation.

The photocatalytic degradation reactions of dyes rhodamine B (RhB) and methyl orange (MO) were carried out in a Pyrex reaction cell. Photocatalyst (1 g L^{-1}) was dispersed in aqueous solution containing given amounts of the pollutants. The suspension was stirred in the dark for 30 min to establish adsorption/desorption equilibrium between the dye and photocatalyst before irradiated by a 300 W Xe lamp (CERAMAX LX-300). The temperature of the reaction solution was maintained at 11 ± 2 °C by a flow of cooling water. The concentration of RhB and MO was monitored by colorimetry with a JASCO V-550 UV–Vis spectrometer. The λ_{max} for RB and MO are 553 and 467 nm, respectively. The UV–Vis DRS after and before degradation showed a decrease of absorbance corresponding to the dye, and the solution became colorless after photocatalytic degradation. Calibration based on the Beer–Lambert law was used to quantify the dye concentration.

3. Results and discussion

3.1. Characterization of the photocatalyst

The TiO_2 nanoparticles possess diameters of approximately 20–50 nm (Fig. 1a), and the cocatalysts, Pt, RuO_2 are highly dispersed on the surface of TiO_2 for Pt–RuO_2/TiO_2 (Fig. 1b). Fig. 1c and d shows the HRTEM images for the microstructure of the catalyst Pt–RuO_2/TiO_2. The image shows that Pt (Fig. 1d) and RuO_2 (Fig. 1d) loaded on TiO_2 are mainly in the form of semispherical particles. The typical particle size of Pt and RuO_2 is estimated to be about 2–5 nm. Both particles are highly dispersed on the surface of TiO_2 (Fig. 1c).

3.2. Photocatalytic oxidation of sulfur-containing organic compounds

3.2.1. The effect of cocatalysts on photocatalytic oxidation of thiophene

Table 1 shows the conversion for photocatalytic oxidation of thiophene on TiO_2 and TiO_2 loaded with various cocatalysts. To study the intrinsic effect of the cocatalyst, the ultra low loading of cocatalyst, 0.01 wt%, was adopted for all the cocatalysts. TiO_2 without the cocatalysts loaded exhibits low conversion for photocatalytic oxidation of thiophene (*ca.* 12%), and the activity was enhanced slightly by loading 0.01 wt% Pt cocatalyst (*ca.* 13%) or 0.01 wt% RuO_2 cocatalyst (*ca.* 21%). Most interestingly, when 0.01 wt% Pt and 0.01 wt% RuO_2 were co-loaded on TiO_2, the conversion was increased to *ca.* 63%, much higher than those of Pt/TiO_2 or RuO_2/TiO_2 and the simple sum of the Pt/TiO_2 and RuO_2/TiO_2 catalysts. TiO_2 co-loaded with Pt and RuO_2 shows strong synergistic

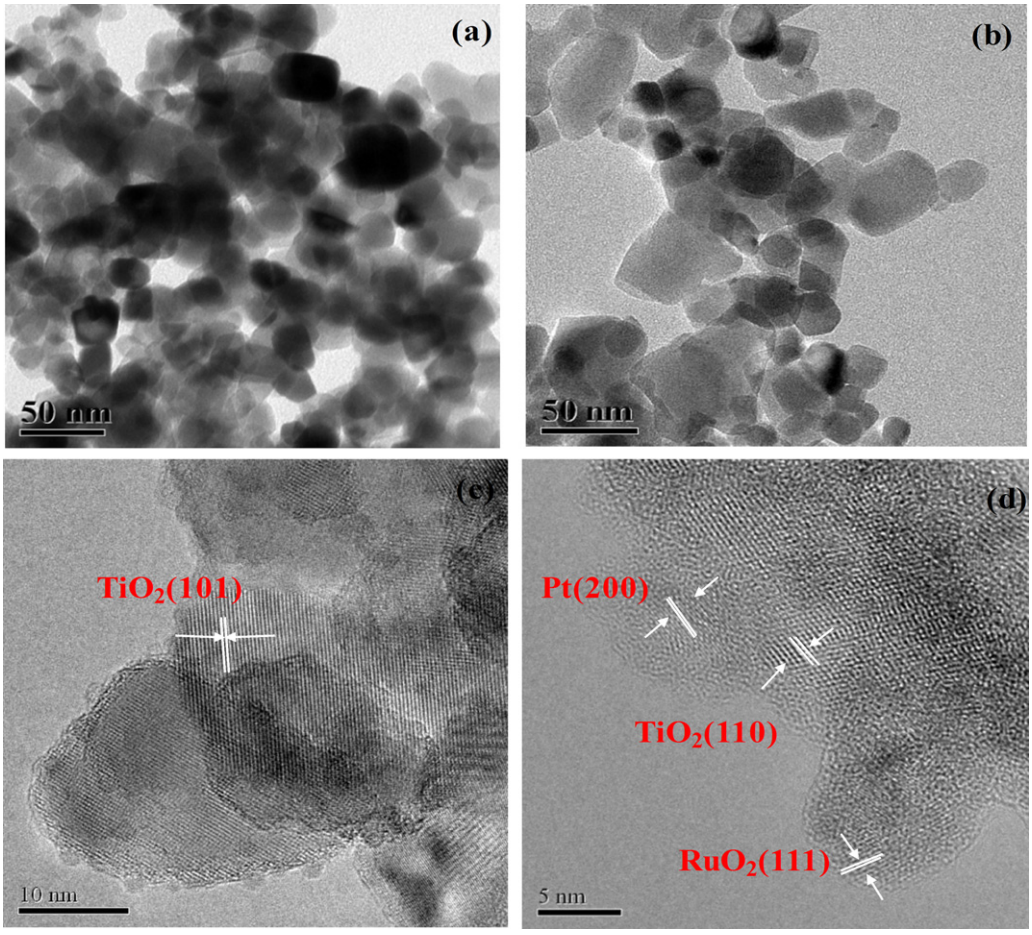

Fig. 1. TEM images of (a) TiO_2, (b) Pt-RuO_2/TiO_2, HRTEM images of (c) and (d) Pt-RuO_2/TiO_2.

effect between the two cocatalysts on the photocatalytic activity of thiophene oxidation. This may be attributed to the suitable energy band matching between the cocatalysts and semiconductor. Compared with TiO_2 loaded with individual cocatalyst, the activity was also improved when Pt and other MO_x (M = Ir, Co, V, Mn, Ni and Fe) were co-loaded on TiO_2, or other noble metals (*e.g.*, Pd, Au, Ni and Cu) and RuO_2 were co-loaded on TiO_2. Above results show that Pt–RuO_2/TiO_2 is the most effective photocatalyst for the photocatalytic oxidation of thiophene. The synergistic effect of cocatalysts on TiO_2 is very favorable for the improvement of photocatalytic activity of thiophene oxidation. Similar to our previous work, the co-loading of Pt and RuO_2 on $ZnGeO_4$, $Y_2Ta_2O_5N_2$ and $BiVO_4$ could result in an enhancement of photocatalytic activity in the photocatalytic water splitting [17,18] and photocatalytic oxidation of thiophene [19].

Table 1
The photocatalytic activity of thiophene oxidation on TiO_2 loaded with various cocatalysts.

Entry	Catalyst	Conv. (%)[a]	Entry	Catalyst	Conv. (%)[a]
1	TiO_2	12	13	NiO_x/TiO_2	20
2	Pt/TiO_2	13	14	Pt–NiO_x/TiO_2	48
3	RuO_2/TiO_2	21	15	FeO_x/TiO_2	15
4	Pt–RuO_2/TiO_2	63	16	Pt–FeO_x/TiO_2	31
5	IrO_x/TiO_2	18	17	Pd/TiO_2	15
6	Pt–IrO_x/TiO_2	45	18	Pd–RuO_2/TiO_2	45
7	CoO_x/TiO_2	15	19	Au/TiO_2	13
8	Pt–CoO_x/TiO_2	33	20	Au–RuO_2/TiO_2	36
9	VO_x/TiO_2	17	21	Ni/TiO_2	16
10	Pt–VO_x/TiO_2	46	22	Ni–RuO_2/TiO_2	26
11	MnO_x/TiO_2	16	23	Cu/TiO_2	13
12	Pt–MnO_x/TiO_2	34	24	Cu–RuO_2/TiO_2	23

[a] Reaction conditions: amount of co-catalysts loaded on TiO_2: 0.01 wt%; the concentration of photocatalyst: 1 g L^{-1}; $[\text{sulfur content}]_{initial}$ = 600 ppm; light source: 300 W Xe lamp (CERAMAX LX-300); O_2 flow: 10 mL min^{-1}; temperature: 11 ± 2 °C; reaction time: 3 h.

From Table 1 and Fig. 2a, we can find that the enhancement of photocatalytic activity by only loading the oxidation cocatalyst RuO_2 is more efficient compared with only loading the reduction cocatalyst Pt. This fact suggests that the oxidation half reaction

Fig. 2a shows the dependence of the conversion for photocatalytic oxidation of thiophene on the loadings of Pt and RuO_2 on TiO_2. For Pt/TiO_2 catalyst, the conversion is slightly increased from 12% to 33% when the loading of Pt varied from 0 to 0.5 wt%. However, the conversion for photocatalytic oxidation of thiophene on RuO_2/TiO_2 shows an obvious different trend. As the loading of RuO_2 increased from 0 to 0.05 wt%, the conversion for photocatalytic oxidation of thiophene was remarkably enhanced to a maximum, 72%. So the loading of RuO_2 (0.05 wt%) was chosen to optimize the conversion for photocatalytic oxidation of thiophene by varying the amount of the cocatalyst Pt. The conversion of thiophene on Pt–RuO_2/TiO_2 shows a similar trend to that of RuO_2/TiO_2, as the loading of co-loaded Pt on RuO_2/TiO_2 was increased, the conversion was markedly enhanced to a maximum, 93% when the loading of Pt is 0.05 wt% (0.05 wt% Pt–0.05 wt% RuO_2/TiO_2). While, the blank experiment without photocatalyst shows only 5% of the conversion of thiophene.

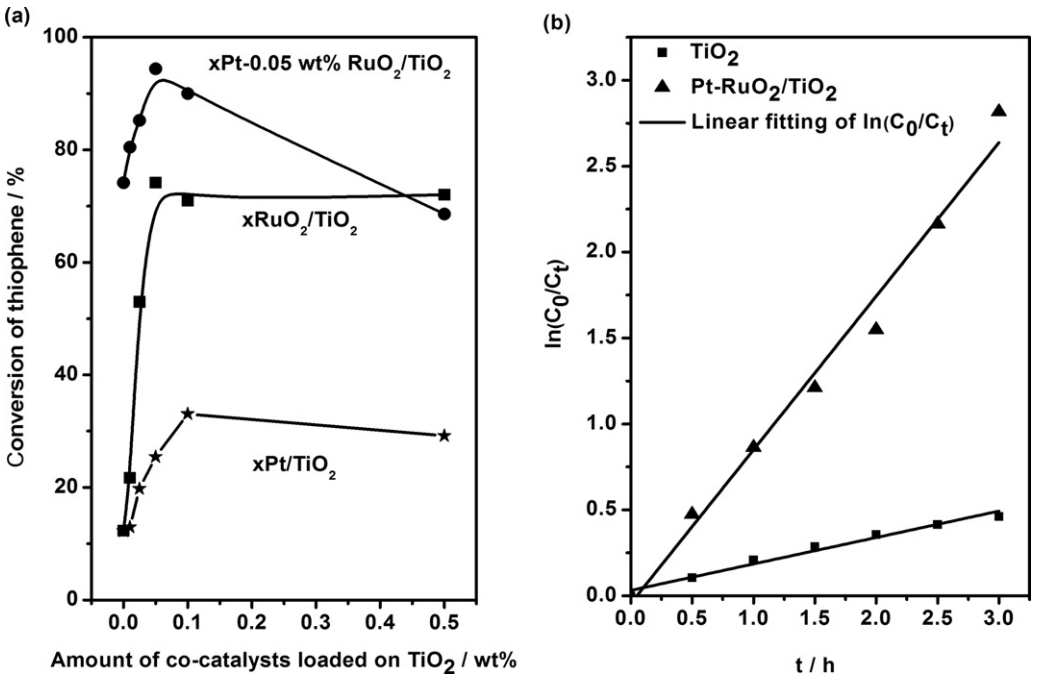

Fig. 2. (a) Photocatalytic activity of thiophene oxidation as a function of the loading amount of Pt alone, RuO_2 alone and co-loaded Pt and RuO_2 on TiO_2. *x* denotes the loading amount of cocatalyst. (b) Variation of $\ln(C_0/C_t)$ *versus* time for the thiophene oxidation on Pt-RuO_2/TiO_2 (▲) and TiO_2 (■). Reaction conditions: the concentration of photocatalyst: 1 g L^{-1}; [sulfur content] initial = 600 ppm; light source: 300 W Xe lamp (CERAMAX LX-300); O_2 flow: 10 mL min^{-1}; temperature: 11 ± 2 °C; reaction time: 3 h.

is the rate determining step in the photocatalytic oxidation of thiophene. The loading of oxidation cocatalyst RuO_2 on TiO_2 is helpful for transferring the photo-generated holes to the surface of photocatalyst, while it is usually difficult for the electron transfer. The loading of reduction cocatalyst Pt is helpful for transferring the photo-generated electrons. Therefore, the effect of only loading oxidation cocatalyst RuO_2 on TiO_2 to enhance the photocatalytic oxidation activity is more obvious compared with only loading the reduction cocatalyst Pt.

3.2.2. The kinetics of photocatalytic oxidation of thiophene

Fig. 2b shows the kinetics of photocatalytic oxidation of thiophene. If the photocatalytic oxidation of thiophene with O_2 as oxidant is a first-order reaction, the sulfur content of the model compound can be expressed as Eq. (1):

$$\ln\left(\frac{C_0}{C_t}\right) = kt \quad (1)$$

where C_0 and C_t are the sulfur content of the model compound at time zero and time t (h), respectively, and k is the first-order rate constant (h^{-1}). Half-life ($t_{1/2}$(h)) can be calculated using Eq. (2):

$$t_{1/2} = \frac{0.693}{k} \quad (2)$$

Fig. 2b illustrates the time-course variation of $\ln(C_0/C_t)$, which is obtained from data shown in Fig. 2a, and k and $t_{1/2}$ are calculated as follows. When TiO_2 was used as the photocatalyst, k and $t_{1/2}$ were 0.15 h^{-1} and 4.62 h, respectively. And k and $t_{1/2}$ were 0.89 h^{-1} and 0.78 h when Pt–RuO_2/TiO_2 was used as the photocatalyst. The results further confirm that the cocatalyst can substantially reduce the activation energy for the photocatalytic oxidation reaction of thiophene.

3.2.3. Photocatalytic oxidation of different sulfur-containing compounds

Fig. 3a shows the photocatalytic oxidation of different sulfur-containing compounds using Pt–RuO_2/TiO_2 catalyst. Ethanethiol, thiophene and benzothiophene were tested. These sulfur-containing compounds, although being different, they can be efficiently oxidized using the 0.05 wt% Pt–0.05 wt% RuO_2/TiO_2 catalyst. To examine the photoproducts, the gas from outlet of the products was introduced to NaOH aqueous solution (0.2 M) for the further analysis. A white precipitate was produced when $Ba(NO_3)_2$ aqueous solution (0.2 M) was added into the NaOH aqueous solution after the reaction (denoted as precipitate 1). Fig. 3b shows the XRD pattern of the white precipitate. The XRD pattern was assigned to $BaCO_3$ which is in good agreement with the standard card of ICDD-PDF No. 05-0378 (space group: Pmcn(62), a = 5.314, b = 8.904, c = 6.430). This result indicates that thiophene can be photocatalytically oxidized to CO_2 and trapped in the NaOH aqueous solution. Very interestingly, when we added HNO_3 (aq) to the precipitate 1, there was still some white precipitate existed which could not be dissolved in HNO_3 (aq), which is denoted as precipitate 2. The XRD pattern of the precipitate 2 shown in Fig. 3b can be readily assigned to $BaSO_4$ which is in good agreement with the standard card of ICDD-PDF No. 24-1035 (space group: Pbnm(62), a = 7.156, b = 8.881, c = 5.454). This indicates that the sulfur in thiophene can be photocatalytically oxidized to SO_3. Namely, thiophene can be oxidized to CO_2 and SO_3 in the photocatalytic oxidation reaction. For ethanethiol and thiophene the main products were identified to be SO_3, however, for benzothiophene the corresponding sulfone was produced as well as SO_3 (Table 2). The sulfur-specific gas chromatography (GC) analysis before and after the photocatalytic oxidation of benzothiophene with molecular oxygen indicates that benzothiophene can be oxidized to corresponding sulfone (Fig. S1). This implies that the photocatalytic oxidation path is different between thiophene and benzothiophene. The intermediate of ethanethiol and thiophene oxidation is relatively unstable, and easy to be further oxidized to SO_3. On the contrary, the corresponding sulfones of BT are relatively stable; as a result, the corresponding sulfones were produced as well as SO_3. The oxidized products, SO_3 and sulfones, can be conveniently removed by washing and extraction processes [20,21].

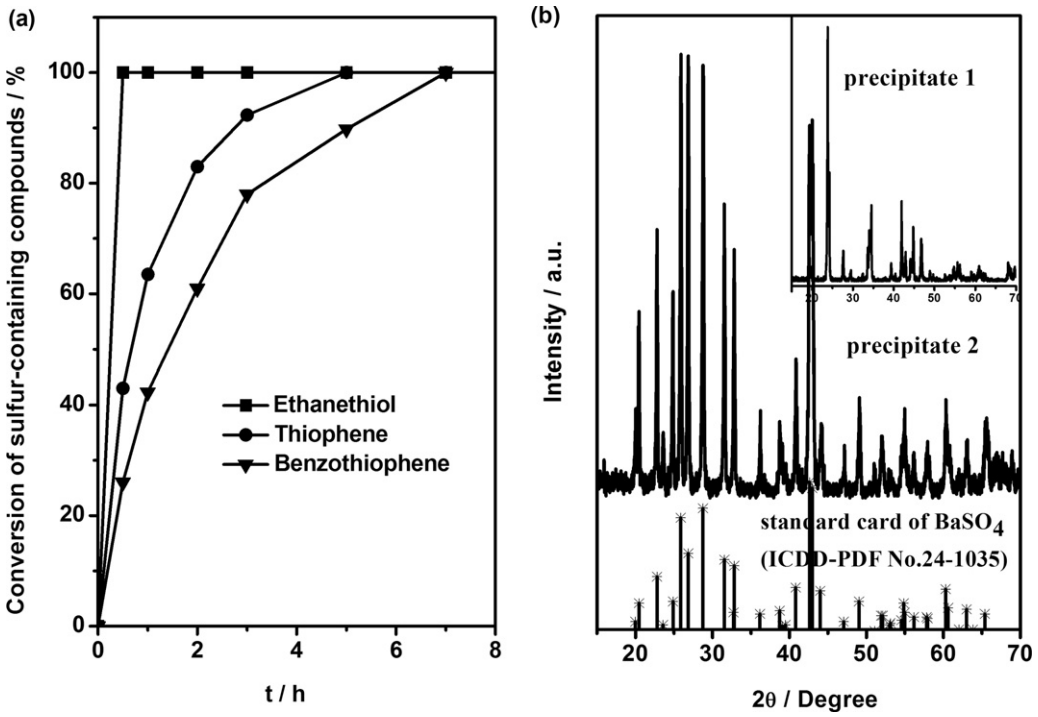

Fig. 3. (a) Photocatalytic oxidation of different sulfur-containing compounds on Pt-RuO_2/TiO_2. Reaction conditions: the concentration of photocatalyst: 1 g L^{-1}; [sulfur content] initial = 600 ppm; light source: 300 W Xe lamp (CERAMAX LX-300); O_2 flow: 10 mL min^{-1}; temperature: 11 ± 2 °C. (b) XRD patterns of the produced precipitates. The inset is the XRD pattern of the precipitate 1. The others are XRD pattern of the precipitate 2 and the standard card of $BaSO_4$ (ICDD-PDF No. 24-1035). The gas produced in the reaction system was absorbed by NaOH aqueous solution (0.2 M), then $Ba(NO_3)_2$ (0.2 M) and HNO_3 (aq) was added successively to produce the precipitate 1 and 2.

3.3. The photocatalytic degradation of rhodamine B (RhB) and methyl orange (MO)

Above results show that the synergistic effect of cocatalysts on TiO_2 is very favorable for the improvement of photocatalytic activity of thiophene oxidation. We further investigate the photocatalytic behaviors for the degradation of rhodamine B (RhB) and methyl orange (MO) dyes to see whether the synergistic effect still exists. Fig. S2a gives the UV–Vis DRS of RhB aqueous solutions with different RhB concentration. RhB has a strong characteristic band at 553 nm. The intensity of the absorption band varies with the variation of RhB concentration. Fig. 4a shows the degradation of RhB aqueous solution on TiO_2, 0.01 wt% Pt/TiO_2, 0.01 wt% RuO_2/TiO_2, 0.02 wt% RuO_2/TiO_2, 0.01 wt% Pt–0.01 wt% RuO_2/TiO_2 and 0.01 wt% Pt–0.02 wt% RuO_2/TiO_2. As shown in Fig. 4a, the activity was enhanced slightly by loading individual cocatalyst Pt or RuO_2. TiO_2 co-loaded with Pt and RuO_2 exhibited much higher photocatalytic activities compared with TiO_2 loaded with individual cocatalyst. Among them, 0.01 wt% Pt–0.02 wt% RuO_2/TiO_2 exhibited highest photocatalytic activity, as it can completely degrade RhB dye in 10 min under irradiation. In contrast, complete oxidation of RhB dye on 0.01 wt% Pt–0.01 wt% RuO_2/TiO_2 requires 20 min, while TiO_2 needed ~45 min. In addition, degradation rate is directly affected by the initial dye concentration. Under same conditions, the time for complete degradation increases with the increase of the initial dye concentration (Fig. 4b). Additionally, Figs. 5 and S3 show the photocatalytic behaviors for degradation of MO. The experimental results for MO degradation under the same conditions clearly indicate that the photocatalytic activity order is consistent with the trend for the RhB degradation. Therefore, these results imply that the photocatalytic activity for degradation of RhB and MO on TiO_2 can be significantly improved by co-loading suitable dual cocatalysts, the synergistic effect between the two cocatalysts on the photocatalytic activity is also very important to the photocatalytic oxidation degradation of dyes.

Table 2
Conversions and products from the photocatalytic oxidation of various sulfur-containing compounds on 0.05 wt% Pt–0.05 wt% RuO_2/TiO_2 photocatalyst in 3 h under irradiation.

Sulfur-containing compounds	Structure	Conversion (%)	Main products detected
Ethanethiol	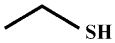	100	$SO_3 + CO_2 + H_2O$
Thiophene		93	$SO_3 + CO_2 + H_2O$
Benzothiophene		78	$SO_3 +$ 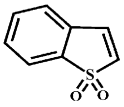

3.4. The ESR measurements and active oxygen species

3.4.1. ESR measurements of the photocatalytic oxidation reaction of thiophene

To clarify the reaction mechanism of photocatalytic oxidation of thiophene and dyes on photocatalysts, we employed the *in situ* ESR spin-trap technique (with DMPO) to probe the active oxygen species generated under the illumination, and simulated the actual reaction condition in the characterization process. Fig. 6 shows a typical ESR spectrum obtained from the *in situ* photocatalytic oxidation reaction of thiophene. No ESR signals were observed either when the photocatalyst was absent or when the reaction was performed with photocatalysts in the dark. After a 10 min of illumination the spectra of the reaction solution in the presence of photocatalysts give a signal centered at $g = 2.0065$, which indicates oxygen involvement [22]. The signals can be assigned to two groups. The characteristic quartet peaks in the presence of photocatalysts TiO_2, Pt/TiO_2, RuO_2/TiO_2 and Pt–RuO_2/TiO_2 is assigned

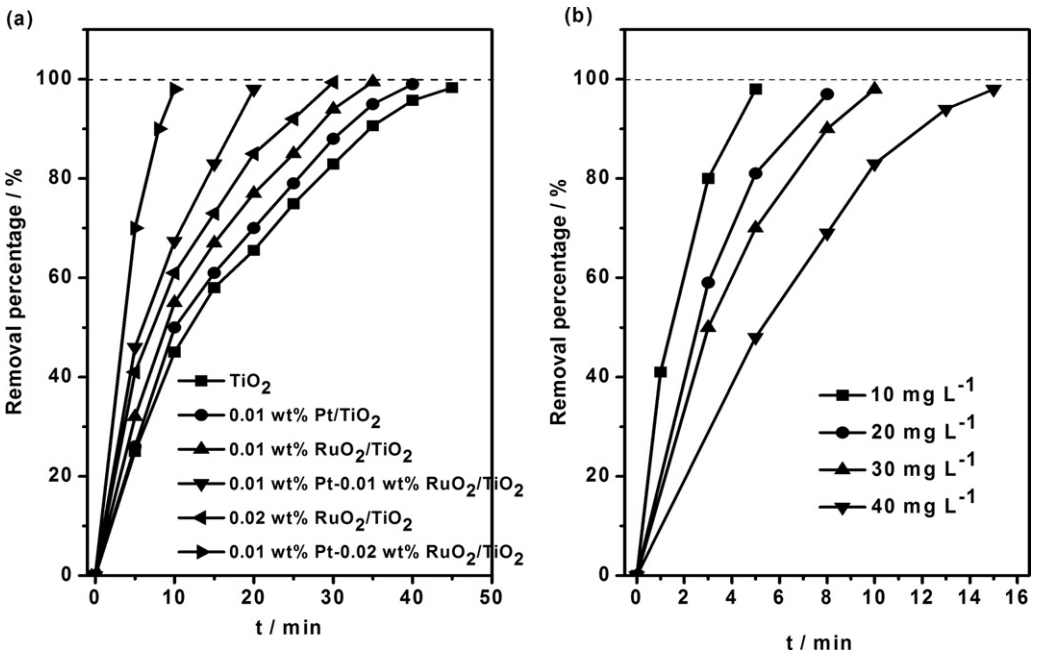

Fig. 4. (a) Photocatalytic oxidation degradation of RhB on TiO_2 and TiO_2 loaded with cocatalysts Pt and RuO_2. Reaction conditions: the concentration of photocatalyst: 1 g L^{-1}; the initial concentration of dye, C_0 = 30 mg L^{-1}; light source: 300 W Xe lamp (CERAMAX LX-300); temperature: 11 ± 2 °C. (b) The photocatalytic oxidation degradation of RhB with different initial concentrations on 0.01 wt% Pt–0.02 wt% RuO_2/TiO_2. Reaction conditions: the concentration of photocatalyst: 1 g L^{-1}; the initial concentration of dye, C_0 = 10 mg L^{-1}; 20 mg L^{-1}; 30 mg L^{-1}; 40 mg L^{-1}; light source: 300 W Xe lamp (CERAMAX LX-300); temperature: 11 ± 2 °C.

to DMPO-OH adduct. The hyperfine splittings are $a_N = a_H = 1.48$ mT, where a_N and a_H denote hyperfine splittings of the nitroxyl nitrogen and *a*-hydrogen, respectively [22]. But the 1:1.4:1.4:1 lineshape is different from the typical 1:2:2:1 lineshape of DMPO-OH adduct, this may be due to the simultaneous presence of DMPO-$O_2^{\bullet-}$. On the other hand, the sextet ESR signal observed along with the characteristic quartet peaks of DMPO-OH is assigned to DMPO-$O_2^{\bullet-}$. And the hyperfine splittings are $a_N = 1.27$ mT, $a_H^{\beta} = 0.99$ mT and $a_H^{\gamma} = 0.14$ mT, where a_N, a_H^{β} and a_H^{γ} denote hyperfine splitting constants of nitroxyl nitrogen, β-hydrogen and γ-hydrogen, respectively [23–26]. Photo-generated electron transfer to O_2 *via* photocatalyst, where superoxide species $O_2^{\bullet-}$ is formed when O_2 reacts with the photo-generated electrons [27]. Additionally, the intensity of the signals is decreased after a 20 min of illumination. This is because of the consumption of the dissolved O_2 and the oxidation of DMPO-OH adduct by h^+ produced during the illumination.

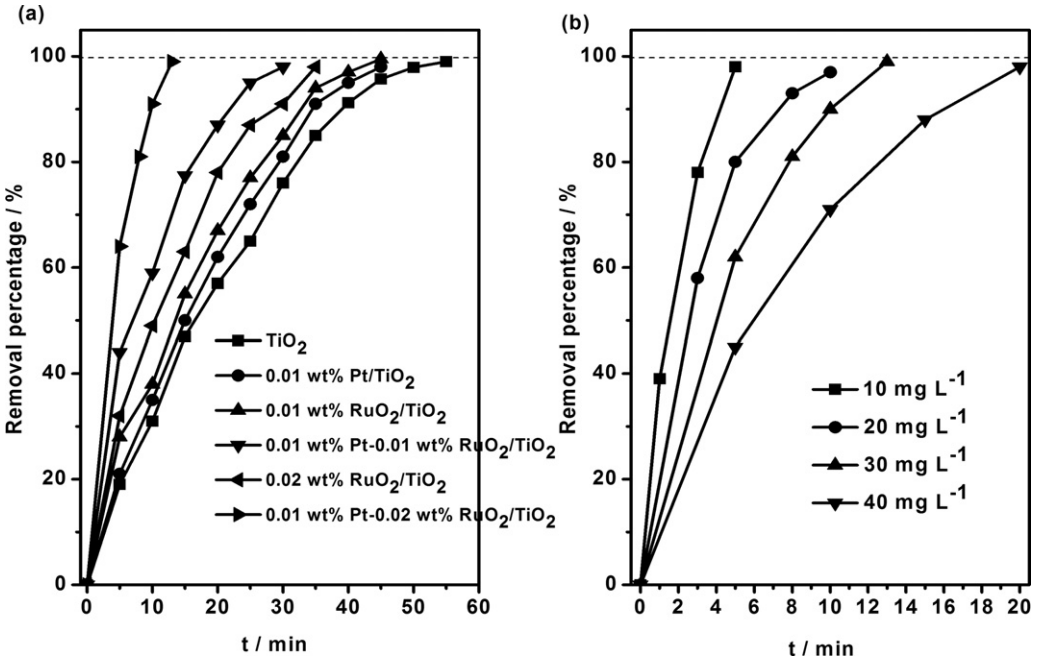

Fig. 5. (a) Photocatalytic oxidation degradation of MO on TiO_2 and TiO_2 loaded with cocatalysts Pt and RuO_2. Reaction conditions: the concentration of photocatalyst: 1 g L^{-1}; the initial concentration of dye, C_0 = 30 mg L^{-1}; light source: 300 W Xe lamp (CERAMAX LX-300); temperature: 11 ± 2 °C. (b) The photocatalytic oxidation degradation of MO with different initial concentrations on 0.01 wt% Pt–0.02 wt% RuO_2/TiO_2. Reaction conditions: the concentration of photocatalyst: 1 g L^{-1}; the initial concentration of dye, C_0 = 10 mg L^{-1}; 20 mg L^{-1}; 30 mg L^{-1}; 40 mg L^{-1}; light source: 300 W Xe lamp (CERAMAX LX-300); temperature: 11 ± 2 °C.

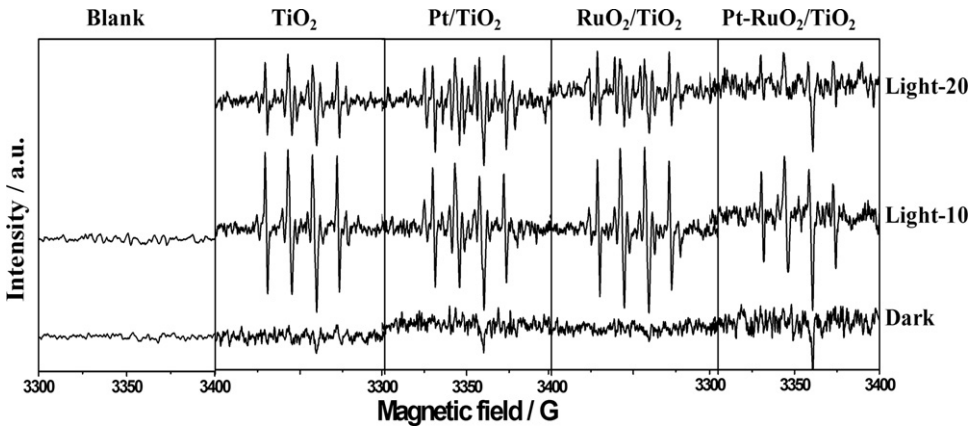

Fig. 6. *In situ* ESR spectra of DMPO-OH and DMPO-$O_2^{\bullet-}$ generated in the photocatalytic oxidation reaction of thiophene with different photocatalysts. The sample tested without photocatalyst is denoted as "Blank". The signals obtained without light irradiation are denoted as "Dark". The signals obtained after irradiating for 10 min are denoted as "Light-10", similarly, 20 min named as "Light-20".

Accordingly, we can conclude that $^{\bullet}OH$ and $O_2^{\bullet-}$ are generated in the presence of photocatalysts under the illumination. Thus the presence of active oxygen species $^{\bullet}OH$ and $O_2^{\bullet-}$ are involved in the photocatalytic oxidation reaction of thiophene.

3.4.2. ESR measurements of the photocatalytic degradation of dyes

Fig. 7 shows the ESR spectra obtained from the *in situ* photocatalytic degradation reaction of dye RhB. No ESR signals are observed either when the photocatalyst is absent or when the reaction is performed with photocatalysts in the dark. After a 2 min of illumination in the presence of photocatalysts a signal centered at $g = 2.0065$ is observed [22]. The characteristic quartet peaks in the presence of photocatalysts TiO_2, Pt/TiO_2, RuO_2/TiO_2 and $Pt–RuO_2/TiO_2$ are assigned to DMPO-OH adduct. The hyperfine splittings are $a_N = a_H = 1.48$ mT, where a_N and a_H denote hyperfine splittings of the nitroxyl nitrogen and *a*-hydrogen, respectively [22]. And the typical 1:2:2:1 lineshape of DMPO-OH adduct is obtained. This provides the evidence of $^{\bullet}OH$ formed in the presence of photocatalysts TiO_2, Pt/TiO_2, RuO_2/TiO_2 and $Pt–RuO_2/TiO_2$ under the illumination. Additionally, the intensity of the characteristic quartet peaks decreased after a 5 min of illumination. This is because of the oxidation of DMPO-OH adduct by h^+ produced during the illumination. Accordingly, we can conclude that $^{\bullet}OH$ was involved in the photocatalytic degradation reaction of dye RhB. From above results, we can find that $O_2^{\bullet-}$ which was involved in the photocatalytic oxidation of thiophene was not generated in the photocatalytic degradation reaction of dye RhB under the illumination. This is due to the low concentration of dissolved O_2 in the reaction system of photocatalytic degradation of RhB. Meanwhile, the rate for the production and consumption of the active oxygen species is faster in photocatalytic degradation reaction of dye RhB than photocatalytic oxidation reaction of thiophene. The reason may be that the aqueous solution is more favorable for the transfer and consumption of active oxygen species.

3.5. The proposed reaction mechanism for the photocatalytic oxidation of pollutants

A schematic description of the mechanism for the photocatalytic oxidation of pollutants (sulfur-containing organic compounds and dyes RhB and MO) on $Pt–RuO_2/TiO_2$ is proposed in Scheme 1. The electron-hole can be separated efficiently by the dual cocatalysts loaded on TiO_2 under the illumination, the adsorbed pollutants

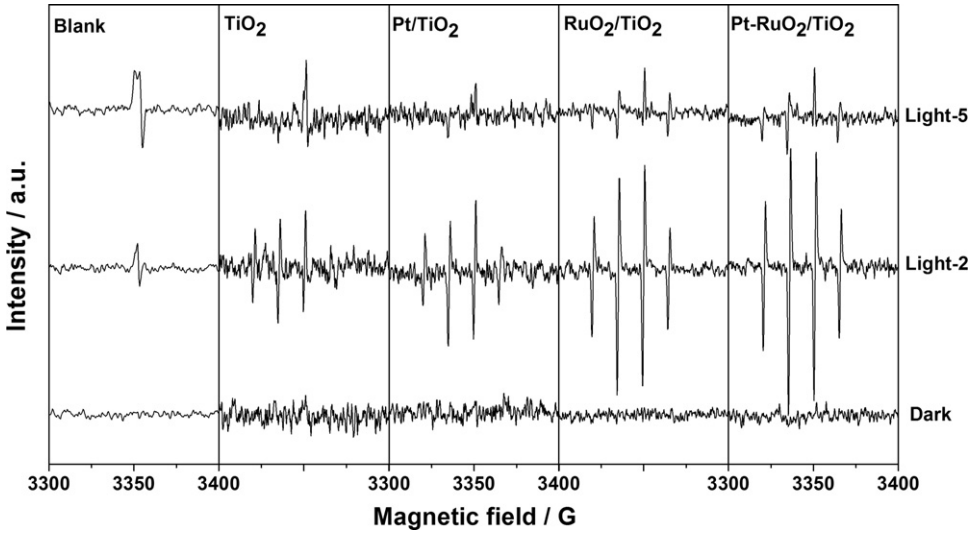

Fig. 7. *In situ* ESR spectra of DMPO-OH generated in the photocatalytic degradation of dye with different photocatalysts. The sample tested without photocatalyst is denoted as "Blank". The signals obtained without light irradiation are denoted as "Dark". The signals obtained after irradiating for 2 min are denoted as "Light-2", similarly, 5 min named as "Light-5".

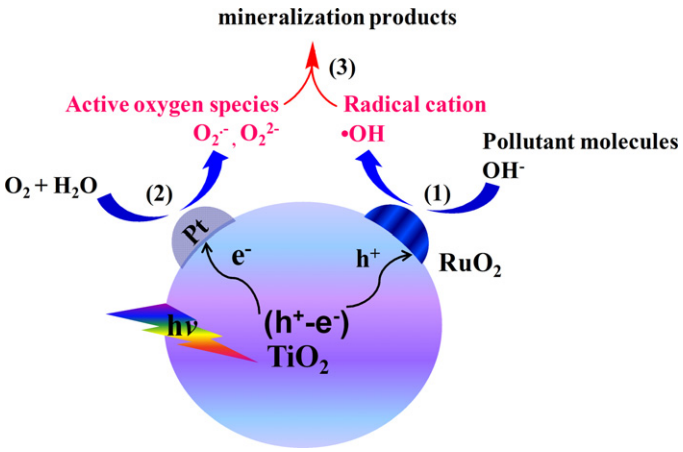

Scheme 1. Schematic description of the mechanism for the photocatalytic oxidation of pollutants on Pt–RuO_2/TiO_2 photocatalyst.

(*e.g.*, thiophene, RhB and MO) readily capture the photo-generated hole transferred *via* RuO_2 cocatalyst to form an unstable oxidized intermediate [28]. •OH is generated *via* the reaction of OH^- with hole in the reaction. On the other side, when O_2 is used as the oxidant, photo-generated electron transfer to O_2 *via* Pt cocatalyst, where superoxide species $O_2^{\bullet-}$ is formed when O_2 reacts with the photo-generated electrons. O_2^{2-}, which is the ESR silent species, also probably formed. Thus, the adsorbed oxygen acts as an electron trap, efficiently inhibiting electron-hole recombination [29]. Consequently, the activation of molecular oxygen and pollutant molecule simultaneously takes place on Pt–RuO_2/TiO_2 catalyst for the photocatalytic oxidation reaction. The interaction of the active oxygen species (•OH, $O_2^{\bullet-}$ and O_2^{2-}) with the pollutant captured the photo-generated hole initiate a series of oxidation reactions. The synergistic effect of RuO_2 acting as an oxidation cocatalyst and Pt acting as a reduction cocatalyst is beneficial for the efficient separation and transfer of the photo-excited electrons and holes [17–19], being responsible for the high photocatalytic oxidation activity for the degradation of pollutants.

4. Conclusions

The sulfur-containing organic compounds, dyes rhodamine B (RhB) and methyl orange (MO) can be efficiently photocatalytically oxidized on TiO_2 co-loaded with less than 0.05 wt% Pt and 0.05 wt% RuO_2 (denoted as Pt–RuO_2/TiO_2). We found that TiO_2 co-loaded with reduction cocatalyst Pt and oxidation cocatalyst RuO_2 shows the considerably synergistic effect between the two cocatalysts on the photocatalytic oxidation activity. This effect has been demonstrated for the photocatalytic oxidation of thiophene and successfully extended to the photocatalytic oxidation of organic dyes. ESR measurements give the evidence for that the active oxygen species (•OH and $O_2^{\bullet-}$) generated by photocatalytic processes are involved in the photocatalytic oxidation of the pollutants. The activation of molecular oxygen and pollutant molecule simultaneously takes place on Pt–RuO_2/TiO_2 catalyst for the photocatalytic oxidation reaction. The results demonstrate that the co-existing oxidation and reduction cocatalysts play a significant role in the photocatalytic oxidation of pollutants. The co-loading of oxidation and reduction cocatalysts is of considerable importance in the designing of highly active photocatalysts for environmental protection.

Acknowledgments

This work was financially supported by National Natural Science Foundation of China (Grant Nos. 20673114, 20973163), National Natural Science Foundation of China (Grant Nos. 21090340/21090341) and Solar Energy Action Plan of the Chinese Academy of Sciences (Grant No. KGCX2-YW-392-1).

Appendix A. Supplementary data

Supplementary data associated with this article can be found, in the online version, at http://dx.doi.org/10.1016/j.apcatb.2012.08.024.

References

[1] M.R. Hoffmann, S.T. Martin, W.Y. Choi, D.W. Bahnemann, Chemical Reviews 95 (1995) 69–96.
[2] A.L. Linsebigler, G. Lu, J.T. Yates Jr., Chemical Reviews 95 (1995) 735–758.
[3] J. Tang, Z. Zou, J. Ye, Angewandte Chemie International Edition 43 (2004) 4463–4466.
[4] D. Chatterjee, S.J. Dasgupta, Journal of Photochemistry and Photobiology C: Photochemistry Review 6 (2005) 186–205.
[5] H.G. Kim, D.W. Hwang, J.S. Lee, Journal of the American Chemical Society 126 (2004) 8912–8913.
[6] T.V. Choudhary, S. Parrott, B. Johnson, Environmental Science and Technology 42 (2008) 1944–1947.
[7] A. Fujishima, T.N. Rao, D.A. Tryk, Journal of Photochemistry and Photobiology C: Photochemistry Review 1 (2000) 1–21.
[8] A. Fujishima, Hashimoto, T. Watanabe, 1st ed., BKC, Inc., Herndon, VA, 1999.
[9] J. Winkler, Macromolecular Symposia 187 (2002) 317–324.
[10] M.A. Fox, M.T. Dulay, Chemical Reviews 93 (1993) 341–357.
[11] J. Ryu, W. Choi, Environmental Science and Technology 42 (2008) 294–300.
[12] T. Ishihara, N.S. Baik, N. Ono, Journal of Photochemistry and Photobiology A 167 (2004) 149–157.
[13] J.W. Tang, Z.G. Zou, J.H. Ye, Angewandte Chemie International Edition 43 (2004) 4463–4466.
[14] M. Yoshida, A. Yamakata, K. Takanabe, J. Kubota, M. Osawa, K. Domen, Journal of the American Chemical Society 131 (2009) 13218–13219.
[15] K. Maeda, R. Abe, K. Domen, Journal of Physical Chemistry C 115 (2011) 3057–3064.
[16] S.S. Dunkle, R.J. Helmich, K.S. Suslick, Journal of Physical Chemistry C 113 (2009) 11980–11983.
[17] M.Y. Liu, W.S. You, Z.B. Lei, G.H. Zhou, J.J. Yang, G.P. Wu, G.J. Ma, G.Y. Luan, T. Takata, M. Hara, K. Domen, C. Li, Chemical Communications 219 (2004) 2–2193.
[18] B. Ma, F. Wen, H. Jiang, J. Yang, P. Ying, C. Li, Catalysis Letters 134 (2010) 78–86.
[19] F. Lin, D.E. Wang, Z.X. Jiang, Y. Ma, J. Li, R.G. Li, C. Li, Energy and Environmental Science 5 (2012) 6400–6406.
[20] B. Lee, Journal of the Air and Waste Management Association 41 (1991) 16–19.
[21] H.Y. Lu, J.B. Gao, Z.X. Jiang, F. Jing, Y.X. Yano, G. Wang, C. Li, Journal of Catalysis 239 (2006) 369–375.
[22] S. Leonard, P.M. Gannett, Y. Rojanasakul, D. Schwegler-Berry, V. Castranova, V. Vallyathan, X.L. Shi, Journal of Inorganic Biochemistry 70 (1998) 239–244.
[23] P. Pieta, A. Petr, W. Kutner, L. Dunsch, Electrochimica Acta 53 (2008) 3412–3415.
[24] J.R. Harbour, M.L. Hair, Advances in Colloid and Interface Science 24 (1986) 103–141.
[25] J.R. Harbour, M.L. Hair, Journal of Physical Chemistry 82 (1978) 1397–1399.
[26] Y. Huang, J. Li, W. Ma, M. Cheng, J. Zhao, J.C. Yu, Journal of Physical Chemistry B 108 (2004) 7263–7270.
[27] Y. Shiraishi, Y. Taki, T. Hirai, I. Komasawaab, Chemical Communications (1998) 2601–2602.
[28] M.A. Fox, A.A. Abdel-wahab, Tetrahedron Letters 31 (1990) 4533–4536.
[29] J. Robertson, T.J. Bandosz, Journal of Colloid and Interface Science 299 (2006) 125–135.